Available online at www.sciencedirect.com
SCIENCE DIRECT®
Organic Electronics 4 (2003) 219–226
Organic Electronics
www.elsevier.com/locate/orgel

Guided electromagnetic waves in organic light emitting diode structures

Thomas Fuhrmann [a,*], Katrin Samse [a], Josef Salbeck [a], Alexandra Perschke [b], Hilmar Franke [b]

[a] *Macromolecular Chemistry and Molecular Materials, Department of Physics, University of Kassel, Heinrich-Plett-Strasse 40, D-34109 Kassel, Germany*

[b] *Laboratory for Applied Physics, Faculty of Science, Gerhard-Mercator-University Duisburg, Lotharstr. 1, D-47048 Duisburg, Germany*

Received 1 August 2002; accepted 3 March 2003

Abstract

A detailed analysis of the optical waveguide modes in organic light emitting diodes (OLEDs) is presented. The modes are compared with respect to their electric field profile, attenuation coefficient and optical confinement factor. The first transversal electric (TE) mode is best suited for an optimized energy transfer from emitting dipoles. The transversal magnetic (TM) modes are characterized by a large plasmon character with high absorption. The propagation constants of distinct modes have been measured in test devices by grating coupling.

PACS: 42.70; 42.82; 78.66
Keywords: Organic light emitting diode; Waveguide; Plasmon; Grating coupler

1. Introduction

According to the principles of quantum electronics, the energy emitted from electronically excited molecules in a thin film multilayer system is distributed among all possible optical modes of the respective frequency [1–3]. If the multilayer system consists of an optical waveguide structure, these modes may be divided into radiative modes which radiate freely into air, substrate modes, and waveguide modes bound within the layer system. Therefore, the rate of spontaneous and stimulated emission can be written as

$$W = \sum_l W_{l,\mathrm{rad}} + \sum_l W_{l,\mathrm{substrate}} + \sum_l W_{l,\mathrm{bound}}$$

and the respective emission rate into each mode l is given in the limit of weak coupling by Fermi's Golden Rule [4].

A typical organic light emitting diode (OLED) usually is a waveguide structure, and much effort has been made to suppress the coupling of energy into waveguide modes in favour of radiation modes in order to increase the output efficiency. On the other hand, for organic lasers or applications in which an OLED is used as a light source for integrated optical circuits, the condition has to

* Corresponding author. Tel.: +49-561-804-4720; fax: +49-561-804-4555.
E-mail address: th.fuhrmann@uni-kassel.de (T. Fuhrmann).

1566-1199/$ - see front matter
doi:10.1016/j.orgel.2003.03.001

be reversed: as much energy as possible should be directed into few distinct waveguide modes. In these modes, stimulated emission is possible due to the enhancement of the emission rate by photons already present in these modes, provided that the gain obtained by excitation exceeds the losses in the waveguide.

In this article, we present an analysis of waveguide modes that occur in typical OLED structures. Of major interest is the question which waveguide mode is best suitable for effective photon feeding by a luminescent layer, i.e. which has the best coupling to light emitters and the least absorption losses. In addition to mode simulations, waveguide coupling experiments which allow experimental access to distinct modes are described.

2. Theory of waveguide modelling

The general structure of an OLED layer system is displayed in Fig. 1. A number of organic layers is placed between an anode, consisting of indium–tin–oxide (ITO) with an isolating SiO_2 underlayer on glass, and a low-work function metal cathode. If organic emission materials with large Stokes shift or low concentrations in a host matrix are chosen, the major contribution to optical absorption is the absorption at the conducting electrodes, which increases towards the infrared region. We chose a red emitting dye (4-(dicyanomethylene)-2-methyl-6-(*p*-dimethylaminostyryl)-4H-pyran) in Alq_3 (aluminum-*tris*(hydroxyquinoline)) as electron transport/emission layer, and AZOPD (*N,N′-bis*(phenyl)-*N,N′-bis*((4-phenylazo)phenyl)benzidine) as hole transport layer, thus confining the emission wavelength to the red (600–640 nm) [5]. For comparison, we also used a transparent layer (Spiro-PBD [6]) as electron transport layer. For all layers we determined the complex refractive index

$$\hat{n} = n + \mathrm{i}k$$

by prism coupling at 632.8 nm (Metricon 2010) and spectroscopic ellipsometry (Woollam VASE). The refractive index data that are given in Fig. 1 have been taken as the material parameters for the simulation.

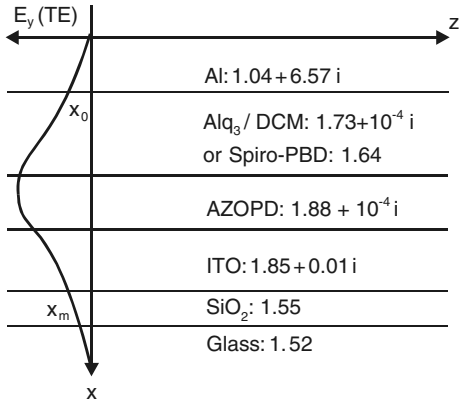

Fig. 1. Definition of the multilayer system used in the simulation and in the experiments.

The calculation of waveguide modes was performed with a transfer matrix method [7,8] using complex refractive indices throughout according to the lossy character of the modes. In each layer, the electric field profile of a mode is written as a superposition of a right-traveling and a left-traveling wave

$$E_i(x) = L_i \exp(-\mathrm{i}k_{ix}(x - x_i)) + R_i \exp(\mathrm{i}k_{ix}(x - x_i)),$$

x being the direction normal to the layers. The corresponding wave vector component is

$$k_{ix} = \frac{\omega}{c}\sqrt{\hat{n}^2 - \hat{n}_{\mathrm{eff}}^2},$$

comprising the complex effective index for mode propagation in z direction which is common for all layers. The field amplitudes for subsequent layers are connected via

$$\begin{pmatrix} R_i \\ L_i \end{pmatrix} = D_{i,i+1} P_{i+1} \begin{pmatrix} R_{i+1} \\ L_{i+1} \end{pmatrix},$$

with propagation matrices

$$P_i = \begin{pmatrix} \exp(-\mathrm{i}k_{ix}(x_i - x_{i-1})) & 0 \\ 0 & \exp(\mathrm{i}k_{ix}(x_i - x_{i-1})) \end{pmatrix}$$

and transmission matrices through the interfaces

$$D_{i,i+1} = \frac{1}{t_{i,i+1}} \begin{pmatrix} 1 & r_{i,i+1} \\ r_{i,i+1} & 1 \end{pmatrix},$$

which are given by Fresnel's formulas. For transversal electric (TE) modes, we have

$$r_{\mathrm{TE}(y)} = \frac{k_{1x} - k_{2x}}{k_{1x} + k_{2x}}, \quad t_{\mathrm{TE}(y)} = \frac{2k_{1x}}{k_{1x} + k_{2x}},$$

whereas for transversal magnetic (TM) modes, we explicitly calculate the field components in both x and z directions, i.e.

$$r_{\mathrm{TM}(x)} = \frac{\hat{n}_2^2 k_{1x} - \hat{n}_1^2 k_{2x}}{\hat{n}_1^2 k_{2x} + \hat{n}_2^2 k_{1x}}, \quad t_{\mathrm{TM}(x)} = \frac{2\hat{n}_1^2 k_{1x}}{\hat{n}_1^2 k_{2x} + \hat{n}_2^2 k_{1x}},$$

$$r_{\mathrm{TM}(z)} = \frac{\hat{n}_1^2 k_{2x} - \hat{n}_2^2 k_{1x}}{\hat{n}_1^2 k_{2x} + \hat{n}_2^2 k_{1x}}, \quad t_{\mathrm{TM}(z)} = \frac{2\hat{n}_1^2 k_{2x}}{\hat{n}_1^2 k_{2x} + \hat{n}_2^2 k_{1x}}.$$

The x component is discontinuous at the interfaces and perpendicular to the Poynting vector, and thus important for energy flux.

Waveguide modes have to fulfill the condition of evanescent fields in the outermost layers

$$\begin{pmatrix} 0 \\ L_0 \end{pmatrix} = \prod_{i=0}^{m} D_{i,i+1} P_{i+1} \begin{pmatrix} R_{m+1} \\ 0 \end{pmatrix} = \begin{pmatrix} m_{11} & m_{12} \\ m_{21} & m_{22} \end{pmatrix} \begin{pmatrix} R_{m+1} \\ 0 \end{pmatrix},$$

which translates into the computational task of finding the minima of $\log|m_{11}/m_{12}|$ by screening the complex plane for the complex mode index $\hat{n}_{\mathrm{eff}}$.

Having found the distinct waveguide modes, the following quantities are calculated for a comparison of different OLED designs:

(i) the attenuation coefficient of the lossy mode $\alpha = \frac{4\pi}{\lambda} \mathrm{Im}\{\hat{n}_{\mathrm{eff}}\}$;

(ii) the fill factor or confinement factor ϵ which is the fraction of mode power lying in the active zone δd which is electron transport/emission layer just at the interface to the hole transport layer. Since exciton diffusion lengths are short, it is assumed to be narrow and given as the differential power of a normalized mode at the emission layer side of the interface, i.e.

$$\varepsilon_{\mathrm{TE}} = \int_{\delta d} E_y^2 \,\mathrm{d}x \Big/ \int_{-\infty}^{\infty} E_y^2 \,\mathrm{d}x \approx E_y^2(x_d)\delta d$$

for TE modes, and

$$\varepsilon_{\mathrm{TM}} = \int_{\delta d} n^2 E_x^2 \,\mathrm{d}x \Big/ \int_{-\infty}^{\infty} n^2 E_x^2 \,\mathrm{d}x \approx n^2 E_x^2(x_d)\delta d$$

for TM modes, respectively.

Since the optical gain is roughly proportional to the fill factor and loss is given by the attenuation coefficient, the ratio ε/α can be taken as a measure for the radiation efficiency of a certain mode.

For all simulations, aluminum and the glass substrate were assumed as boundary half-spaces. The SiO_2 thickness was fixed to 23 nm, different ITO thicknesses between 20 and 300 nm were used, and the thicknesses of the organic layers were varied in a wide range, up to the occurrence of four modes (two TE-polarized, two TM-polarized).

3. Simulation results and discussion

The mode profiles of a representative sample structure large enough to allow the comparison of four modes is shown in Fig. 2. In the following, the general features of each mode is discussed.

3.1. The TE_0 mode

The fundamental TE_0 mode is the only mode that exhibits one intensity maximum located in the center of the device. It is guided by the high refractive indices of ITO and the hole transport layer. The overall width of the profile is controlled by the effective index of the mode: High effective indices obtained for large device thicknesses give smaller mode profiles.

From a detailed comparison of different devices we derived the following conclusions. A thin ITO layer is advantageous because of two reasons: it decreases the absorption and it shifts the mode maximum further towards the emission zone, resulting in a better confinement factor. The mode maximum can be placed still nearer to the emission zone by reducing the thickness of the hole transport layer (Fig. 3(b)), up to an optimum confinement factor for hole transporting layers between 50 and 150 nm. On the other hand, this is accompanied by an increase of the attenuation coefficient (Fig. 3(a)). The best ε/α ratios can be obtained for AZOPD layer thicknesses of 300 nm. Increasing the electron transport/emission layer thickness improves both absorption behaviour and confinement, although there is a practical limit due to the requirement of balanced charge transport.

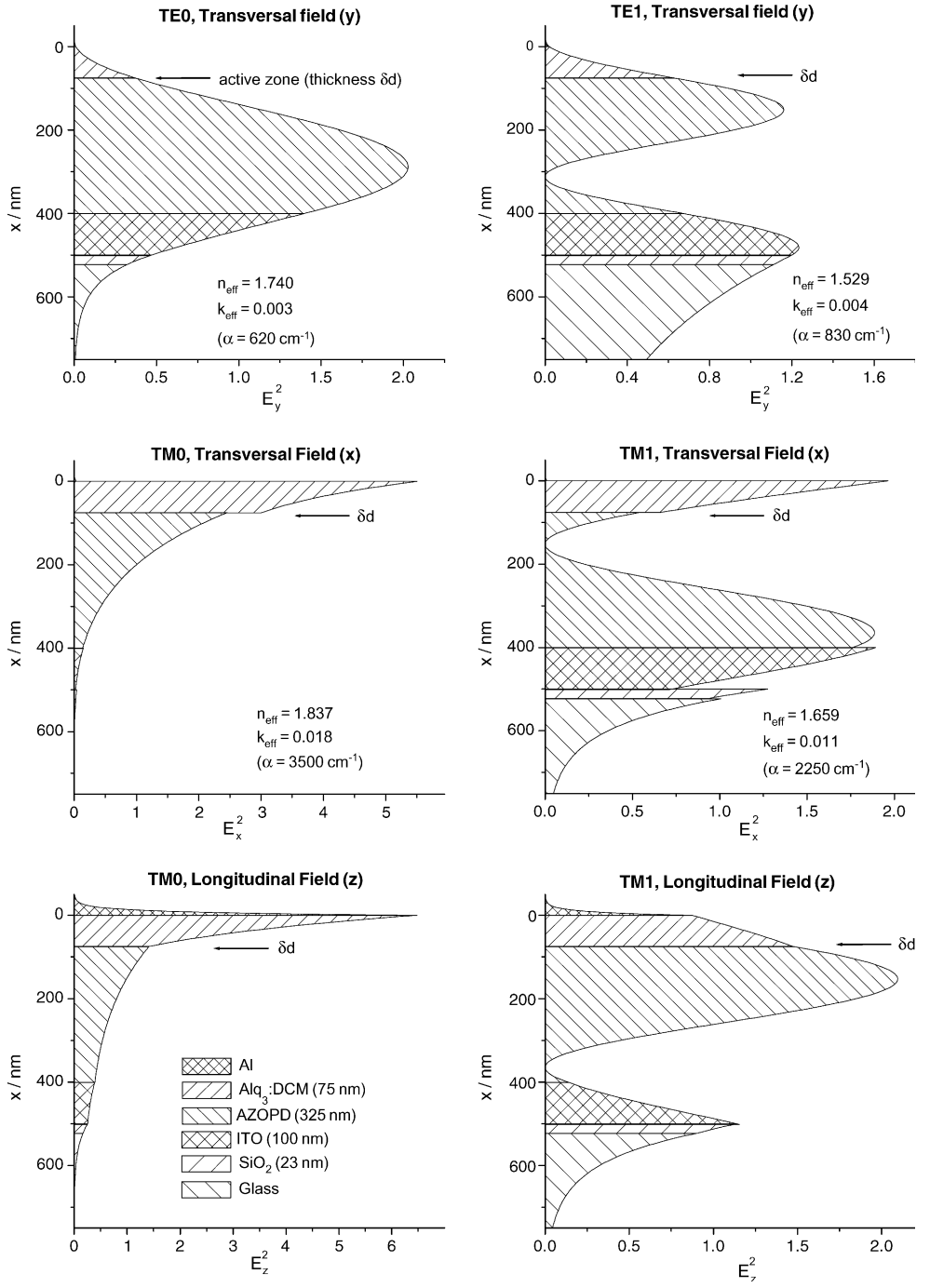

Fig. 2. Mode profiles of a sample device allowing four different modes (composition: Al/Alq_3: DCM 75 nm, AZOPD 325 nm, ITO 100 nm, SiO_2 23 nm, glass): plotted are the transverse electric field for the TE modes and the reverse and longitudinal field components for the TM modes.

Generally, TE_0 modes exhibit a lower attenuation than other waveguide modes. Attenuation coefficients lower than 100 cm^{-1} can be obtained.

3.2. The TE_1 mode

The second TE mode is generally broader than the TE_0 mode because of its smaller effective index and the field amplitude node in the center of the structure. It exists only in relatively thick layers, which are unfavourable for charge transport and thus probably unsuitable for OLEDs. The only interesting exception are devices with thick ITO layers which of course contribute to the overall thickness, thus reducing the need for thick organic layers. By a balanced layer design, the first maximum of the profile can be placed close to the emission zone, the second one then being concentrated at the ITO layer. Depending on the relative layer thicknesses, the amplitudes can be adjusted in a way that most intensity is concentrated at the emission zone maximum. Because of the orthogonality of the modes, this means that the TE_0 mode is then mainly concentrated on the ITO side. Such favourable mode profiles with high confinement factor and low absorption can be achieved with the help of an additional low index layer between AZOPD and ITO (Fig. 4).

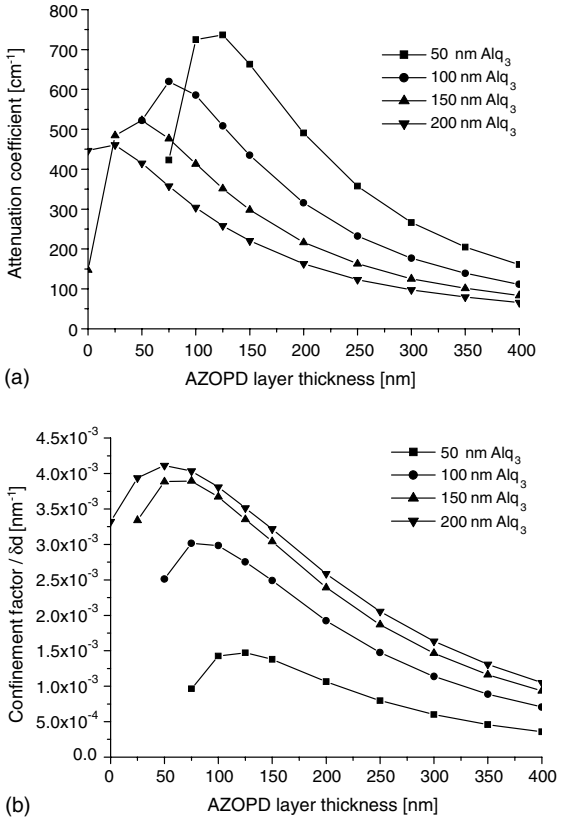

Fig. 3. Attenuation coefficient and confinement factor for the TE_0 mode for different layer thicknesses of AZOPD and Alq_3. The thickness of the ITO layer was 20 nm for all simulations.

3.3. The TM_0 mode

Contrary to dielectric waveguides, the first TM mode in OLEDs has a higher effective index as the TE_0 mode and is essentially a surface plasmon mode at the cathode surface. The importance of surface plasmons in OLEDs has been pointed out recently [9]. Since the TM_0 mode has its maximum at the cathode interface, the confinement factor is quite high, provided that the electron transport/emission layer is not too thick. On the other hand, the plasmon modes exhibit a high absorption, the attenuation coefficient being one order of magnitude higher than for TE modes. Typical values are $\alpha = 2000$–4000 cm^{-1}. This absorption cannot be

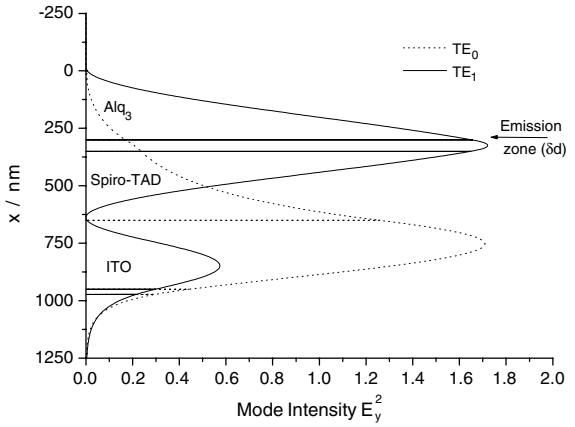

Fig. 4. Optimization of a TE_1 mode by inserting an additional hole transporting layer ($n = 1.74$, Spiro-TAD [6]). The TE_0 mode is centered at the ITO layer ($\cdots$), the orthogonal TE_1 mode has its maximum near to the emission zone. Relatively large thicknesses are required (Alq_3 300 nm, AZOPD 50 nm, Spiro-TAD 300 nm, ITO 300 nm).

compensated by the higher confinement factor which can be concluded from the smaller ε/α ratios in comparison with TE_0 modes. Recent experiments show, however, that plasmon modes can be used for efficient transmission through otherwise opaque metal layers by surface plasmon cross coupling which is a very interesting application of this mode [10].

3.4. The TM_1 mode

The TM_1 mode is a waveguide mode concentrated mainly on the high index layers, but retains some plasmon character due to the coupling via the Alq_3 layer with finite thickness. In Fig. 5, it is shown how the effective indices of the TM_0 and TM_1 modes change with increased coupling. It should be pointed out here, that the order of the plasmon-type and waveguide-type modes may be reversed, if the uncoupled plasmon mode index is relatively low, which occurs for low-index electron transport layers (e.g. if using Spiro-PBD instead of Alq_3, see below).

In the TM_1 mode, the variation of polarization across the mode profile is very pronounced (Fig. 2). In the hole transport layer, near to the emission zone, it is completely z-polarized, which is unfavourable for energy coupling, whereas at the ITO side it is completely x-polarized. Low confinement and high absorption—even if not so high as in the TM_0 mode—makes this mode not suitable for efficient energy transfer from the emission zone.

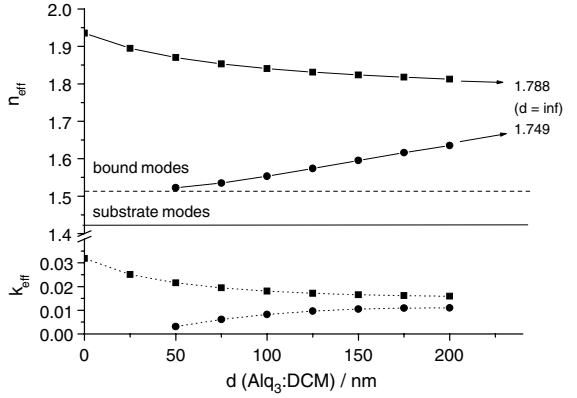

Fig. 5. Coupling of the plasmon mode and the first TM waveguide mode by varying the electron transport layer thickness. Shown are the real and imaginary part of the effective indices. The uncoupled mode indices are $1.788 - 0.020i$ for the Al/Alq_3 interface plasmon and $1.749 - 0.0003i$ for the Alq_3/200 nm AZOPD/20 nm ITO waveguide.

4. Experimental determination of modes

The presence of distinct modes for a certain wavelength can be measured by a waveguide coupling experiment, either prism coupling or grating coupling. We used grating coupling as a non-contact method by holographic grating patterning of the hole transporting layer with a grating constant of 665 nm. Details on the material and the patterning technique can be found elsewhere [5,11]. The implemented grating is a small perturbation of the waveguide and couples the waveguide modes to distinct radiation modes with the condition

$$\sin\theta = n_{\text{eff}} - m\frac{\lambda}{\Lambda}$$

(θ: angle of incidence; m: coupling order; λ: wavelength; Λ: grating constant).

In angle-dependent transmission measurements at a certain wavelength (Fig. 6), the modes appear as a sharp transmission drop at angles that fulfill the coupling condition. By this method, the position of the modes can be tracked at subsequent depositions of the layers. In Fig. 7, this is shown for a sample device, for which a 230 nm layer of Spiro-PBD and then 15 nm aluminum was evaporated on a prestructured sample, consisting of glass substrate, 70 nm SiO_2, 25 nm ITO, and 425 nm AZOPD. The mode indices were measured at a test wavelength of 632.8 nm. After deposition of several 100 nm of the Spiro-PBD layer, the mode indices do not change any more upon increasing this layer thickness further, which means that the low-index electron transport layer acts as a cladding layer to the ITO/AZOPD waveguide core. Similarly, the evaporation of aluminum does not effect the TE modes substantially, whereas the TM modes are changed due to coupling with the surface plasmon. The surface plasmon of a pure Al/Spiro-PBD interface would be at $n_{\text{eff}} = 1.69$, which is lower than the highest TM mode of the unme-

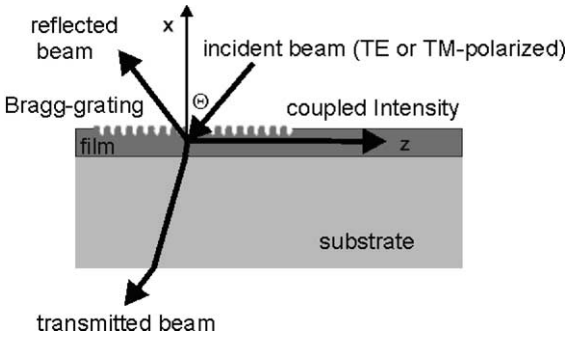

Fig. 6. Setup for mode index measurement by grating coupling. Some intensity of the incident beam is coupled into a forward or backward traveling waveguide mode, depending on the coupling condition. The transmitted beam is monitored. For the experiments, a HeNe laser operating at 632.8 nm was used as the light source. The grating period was 665 nm.

tallized layer system and means that it becomes the *second* TM mode in the complete device. This can be seen in the experiment from the width of the resonances: the second peak is broadened with respect to the other two, thus indicating a mode with stronger absorption.

5. Conclusion

We showed the characteristic features of waveguide modes that occur in multilayer films with the layer structure of OLEDs, and demonstrated experimental access to exciting these modes and extracting energy from them. In each mode, energy from excited molecules can coupled in, but the efficiencies depend strongly on confinement factors and mode attenuation coefficients. If light is to be directed into waveguide modes, the TE_0 mode seems to be the most suitable, since the overall layer thickness can be kept thin, and the plasmon interaction is low.

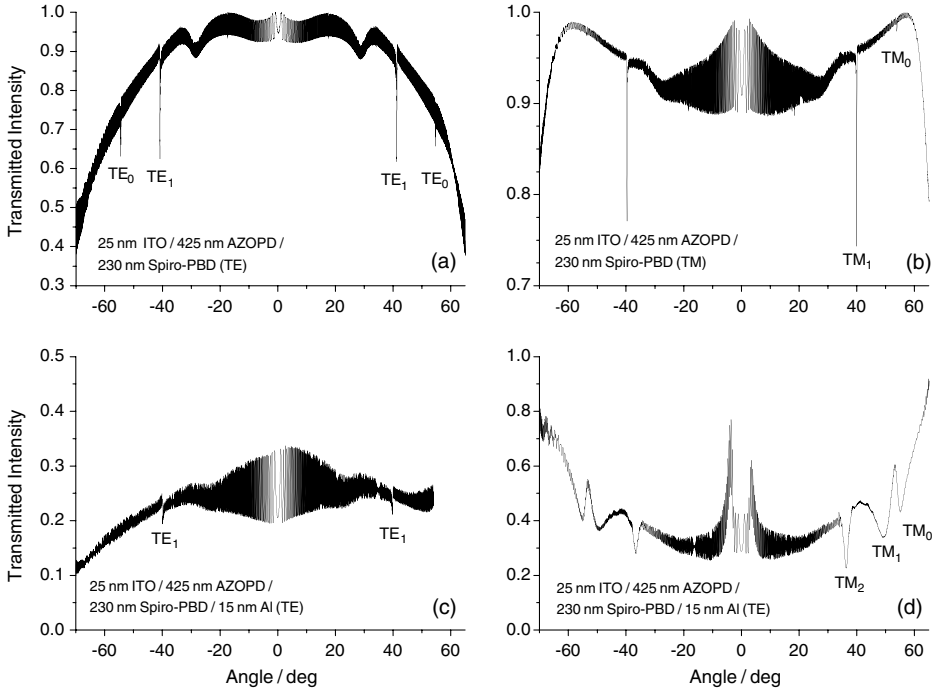

Fig. 7. (a) Grating coupling results (TE polarization) for a device with the structure glass substrate/70 nm SiO_2/25 nm ITO/425 nm AZOPD/230 nm Spiro-PBD, (b) the same device measured in TM polarization, (c) and (d) measurements after deposition of 15 nm aluminum on the device. The TE modes are barely visible after aluminum deposition. In TM polarization, the additional mode with surface plasmon character occurs as the second TM mode.

Acknowledgements

This work was supported by the German Ministry of Education and Research (BMBF) under contract no. 03N 8603. We thank Ansgar Draude, Nils Reinke and Siegfried Kirsch for experimental support.

References

[1] W. Lukosz, Phys. Rev. B 22 (1980) 3030.
[2] C.F. Janz, J.N. McMullin, IEEE Quantum Electr. 31 (1995) 1344.
[3] H.P. Urbach, G.L.J.A. Rikken, Phys. Rev. A 57 (1998) 3913.
[4] A. Yariv, Quantum Electronics, third ed., John Wiley & Sons, New York, 1988.
[5] T. Fuhrmann, T. Tsutsui, Chem. Mater. 11 (1999) 2226.
[6] J. Salbeck, N. Yu, J. Bauer, F. Weissörtel, H. Bestgen, Synth. Met. 91 (1997) 209.
[7] J. Carroll, J. Whiteaway, D. Plumb, Distributed Feedback Semiconductor Lasers, SPIE Press, 1998.
[8] P. Yeh, Optical Waves in Layered Media, John Wiley & Sons, New York, 1988.
[9] P.A. Hobson, J.A.E. Wasey, I. Sage, W.L. Barnes, IEEE Selected Topics Quantum Electr. 8 (2002) 378.
[10] D.K. Gifford, D.G. Hall, Appl. Phys. Lett. 80 (2002) 3679.
[11] A. Perschke, T. Fuhrmann, Adv. Mater. 14 (2002) 841.